Bat Flight Generates Complex Aerodynamic Tracks

A. Hedenström, *et al.*

Science **316**, 894 (2007);
DOI: 10.1126/science.1142281

Science (print ISSN 0036-8075; online ISSN 1095-9203) is published weekly, except the last week in December, by the American Association for the Advancement of Science, 1200 New York Avenue NW, Washington, DC 20005.

assistance of many colleagues involved in sample collection, phenotyping, and DNA extraction in all the different studies. We thank K. Parnell, C. Kimber, A. Murray, K. Northstone, and C. Boustred for technical assistance. We thank S. Howell, M. Murphy, and A. Wilson (Diabetes UK) for their long-term support for these studies. We also acknowledge the efforts of J. Collier, P. Robinson, S. Asquith, and others at Kbiosciences.

Accession numbers for deposited sequence variants from dbSNP are Exon3_A 69374768, 3_UTR_A 69374769, 3_UTR_B 69374770, and 3_UTR_G 69374771.

Supporting Online Material
www.sciencemag.org/cgi/content/full/1141634/DC1
Materials and Methods
SOM Text
Figs. S1 to S3
Tables S1 to S4
References

22 February 2007; accepted 6 April 2007
Published online 12 April 2007;
10.1126/science.1141634
Include this information when citing this paper.

Bat Flight Generates Complex Aerodynamic Tracks

A. Hedenström,[1]* L. C. Johansson,[1] M. Wolf,[1] R. von Busse,[2] Y. Winter,[2,3]† G. R. Spedding[4]

The flapping flight of animals generates an aerodynamic footprint as a time-varying vortex wake in which the rate of momentum change represents the aerodynamic force. We showed that the wakes of a small bat species differ from those of birds in some important respects. In our bats, each wing generated its own vortex loop. Also, at moderate and high flight speeds, the circulation on the outer (hand) wing and the arm wing differed in sign during the upstroke, resulting in negative lift on the hand wing and positive lift on the arm wing. Our interpretations of the unsteady aerodynamic performance and function of membranous-winged, flapping flight should change modeling strategies for the study of equivalent natural and engineered flying devices.

Bats and birds represent two independent evolutionary pathways solving the same problem: powered vertebrate flight. The smaller species show similar wing morphology, kinematics, and flight speeds and operate at similar Reynolds number (*1*). However, the wings of bats and birds also differ in some important respects. For example, the primary feathers of a bird wing can be separated so air can pass through as in a Venetian blind to produce a feathered (and aerodynamically inactive) upstroke. Although bat wing membranes can be actively stretched and collapsed (*2*), they probably cannot be made aerodynamically inactive as easily as bird wing feathers. Flapping wings generate trailing vortices containing information about the time-history and magnitude of the aerodynamic force produced during the wingbeat, and so wake vortices act as an aerodynamic footprint marking the previous passage of the animal through the air (*3*–*10*). The equivalence of forces exerted between a solid object and the surrounding fluid is a consequence of Newton's laws and has long been exploited to estimate drag forces from wake momentum fluxes (*11*, *12*). Similarly, for a lifting body immersed in a uniform flow of speed U, the aerodynamic lift per unit of span can be written as $L' = \rho U \Gamma$, where ρ is air density and Γ is the circulation on the wing section. In the absence of viscosity, vorticity and circulation are conserved according to Helmholtz's laws, and so any change in aerodynamic force (and hence circulation on the wing) must be associated with the shedding into the wake of vorticity of opposite sign, whose circulation matches the change on the wing.

The wake vortices of three bird species have recently been studied in some detail across wide speed ranges (*8*, *10*, *13*), whereas those of bats have received comparatively little attention (*6*). In the one qualitative study of airflows behind bats passing through a bubble cloud (*6*), the bats were reported to generate single vortex loops from each downstroke (with an inactive upstroke) at slow speed, whereas at a faster cruising speed, a pair of undulating vortices trailed the path of the wingtips throughout the wingbeat, implying that the upstroke generated lift. However, kinematic studies show a wingtip reversal during the upstroke during hovering and slow speed in bats (*14*–*19*), suggesting a reversal of the wing circulation during the upstroke, whose signature should be observable in the wake.

We made a systematic and quantitative study of the variation in wake topology and relative down- and upstroke function with flight speed in a small nectar-feeding phyllostomid bat species, *Glossophaga soricina*. Although detailed kinematics data are available for this species across a speed range from 1.2 to 7.5 m/s (*19*), it is impossible to infer the wake vortex distribution from kinematics alone (*19*). The aim was also to test the hypotheses, based on kinematics, that (i) the backward flick of the wing at slow speeds, as inferred on the basis of kinematics, generates lift and thrust (*14*, *16*, *17*, *19*); and (ii) that the negative angle of attack during the upstroke at moderate speeds generates negative lift (*14*, *16*, *19*). Images of the wake were analyzed by means of a digital particle image velocimetry (DPIV) method, and the quantitative measures of wake vorticity and total circulation were used to deduce the magnitude of aerodynamic forces and construct the wake topology (*20*).

We studied the wakes generated by two adult *G. soricina* individuals across the speed range from 1.5 to 7 m/s [body mass, 11 g; wingspan, 0.24 m; aspect ratio, 6.3 (*21*); Reynolds number (Re) $\approx 4 \times 10^3$ to 18×10^3; Strouhal number (St) ≈ 0.27 to 0.81 (*22*)]. Two orientations of the image plane were used: (i) a vertical streamwise plane aligned with the flow at three different positions along the wing span (outer wing, inner wing, and mid-body), and (ii) a cross-stream plane aligned perpendicular to the flow direction (Trefftz plane) (*20*).

We focus our presentation of the wakes on slow (1.5 m/s), medium (4 m/s), and high (6.5 m/s) speeds, which cover the natural range of forward speeds (*19*, *23*). At slow speed (top row of Fig. 1), a strong start vortex, formed at the beginning of the downstroke, can be seen across the span (red blobs at right in Fig. 1, A to C, marked 1 in Fig. 1A). At the transition from downstroke to upstroke, the wing goes through a large supination (pitch-up rotation), so that the wing is flipped upside down. At this point, a combined stop-and-start vortex is shed (blue blob, left side of Fig. 1, A to C). During the upstroke, the wing moves backward faster than the forward speed, with circulation reversed, and the induced flow in the wake is primarily a backward-directed jet. Thus, the net aerodynamic force is forward (thrust) and upward (lift). At the following transition from upstroke to downstroke, the wings pronate rapidly (a pitch-down rotation), to shed a combined start/stop vortex for the next downstroke. This start/stop vortex (2 in Fig. 1A) appears above the previous one (1 in Fig. 1A) because the wake has convected downward in the interim. At the higher flight speed of 4 m/s, illustrated in the next two rows of Fig. 1 (panels D to F for downstroke and G to I for upstroke), the wake structure is quite different. The downstroke generates a strong start vortex (red patches in Fig. 1, D to F). The corresponding stop vortex is weaker and more diffuse, increasingly so as we move from outer wing (Fig. 1D) to inner wing (Fig. 1E) and body (Fig. 1F) image planes. Trace amounts of negative (blue) vorticity can be seen throughout the wingstroke. The associated induced velocity field (vectors in Fig. 1, D to F) shows a downward- and backward-directed momentum

[1]Department of Theoretical Ecology, Lund University, SE-223 62 Lund, Sweden. [2]Department of Biology, University of Munich, Germany. [3]Max-Planck Institute for Ornithology, Seewiesen, Germany. [4]Department of Aerospace and Mechanical Engineering, University of Southern California, Los Angeles, CA 90089–1191, USA.

*To whom correspondence should be addressed. E-mail: anders.hedenstrom@teorekol.lu.se

†Present address: Department of Biology, Bielefeld University, D-335 01 Bielefeld, Germany.

jet whose reaction force on the wings will be lift and thrust.

At 4 m/s, the upstroke generates lift as demonstrated by the downward flow in Fig. 1, H and I. As the wing is flexed on the upstroke, the outer wing image plane (Fig. 1G) now cuts through the outer part of the trailing wingtip vortex, which has a flow curling upward around the trailing vortex. The transition from lifting upstroke to downstroke is marked by a feature seen in Fig. 1, E, F, H, and I, where a substantial upward flow appears to the right of the strong start vortex. At the mid-body position (Fig. 1F), there is also a stronger flow in the flight direction, from right to left. The start vortex is weaker here than at corresponding points in the wing cycle but further out on the wing (Fig. 1, D and E). It is clear that at the inner wing, some kind of secondary vortex shedding has occurred, one that is associated with drag and negative lift.

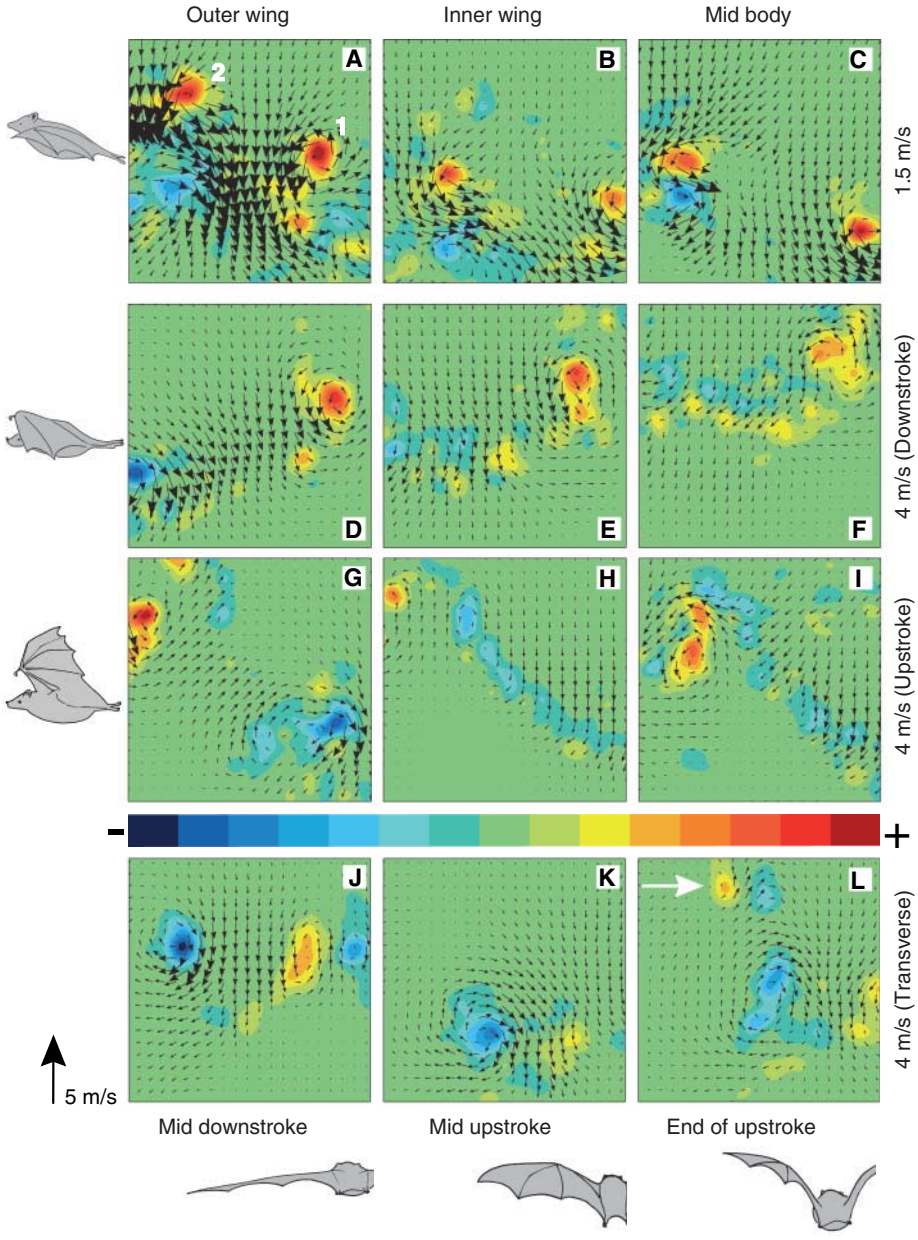

Fig. 1. Color-coded vorticity fields from a bat flying in a wind tunnel (see also fig. S3). Flight direction is from right to left for the upper nine panels, as indicated by the bat silhouettes to the left. The upper nine panels show spanwise vorticity (ω_y) from image planes aligned with the flow [the *x-z* plane (fig. S1)], at positions directly downstream from the outer wing (column 1), inner wing (column 2), and body (column 3), and at 1.5 m/s (**A** to **C**) and 4 m/s (**D** to **I**), respectively (further details in fig. S2). At 1.5 m/s, an entire wingstroke is captured on one frame, but at 4 m/s, separate frames show the downstroke [(D) to (F)] and upstroke [(G) to (I)] because the wingbeat wavelength increases with increasing speed. The bottom row (**J** to **L**) shows streamwise vorticity (ω_x) from the transverse image plane [*y-z* (fig. S1)]. Each transverse image covers the left wing and the body, as indicated by the bat silhouettes below. In (L), a white arrow indicates the vortex shed from the outer wing at the end of the upstroke. The color scale symmetrically represents variation in vorticity (per second) as follows: top row, −450 minimum, 450 maximum; second, third, and fourth rows, −300 minimum, 300 maximum. Velocity vectors are scaled to the reference vector (5 m/s) at bottom left. Each panel covers an area measuring 19.5 × 19.5 cm^2.

Further evidence comes from transverse planes that cut across the wake in Fig. 1, J to L (bottom row). In both mid-downstroke (Fig. 1J) and mid-upstroke (Fig. 1K), although the major feature is an induced downwash that characterizes a lifting body, there is also a streamwise vortex of opposite sign (yellow patch), shed toward the wing root (fig. S3). The horizontal distance between tip vortex (blue) and root vortex (yellow) is reduced as the wings are flexed on the upstroke. At the end of the upstroke, the streamwise vorticity (Fig. 1L) shows another secondary flow at the top of the image (white arrow; see also Fig. 1G above and to the right of the red start vortex). This is a vortex dipole structure with opposite sense to the main vortex: The yellow patch is outboard of the blue patch and the induced flow is upward. The circulation on the outer, hand wing has been reversed, and kinematic measurements show that it has a negative aerodynamic angle of attack here (fig. S4). At a flight speed of 6.5 m/s, the wake is qualitatively similar to that at 4 m/s, but the strength of the vortices is reduced and the wake wavelength is increased (fig. S3).

A full-span transverse image from the mid-downstroke wake (Fig. 2) summarizes one moment in the wingbeat and clearly shows the cores of the wingtip vortices and the opposing vorticity near the wing base. The strength of the wing base vortex is approximately 50% of that of the tip vortex, and it is evident that the three-dimensional wake structure over the entire wingbeat will be substantially more complex than realized hitherto. Nevertheless, certain quantitative measures reveal a quite orderly progression of wake vortex strengths with flight speed.

The magnitude of circulation of the strongest start and stop vortices in the wake decreases monotonically with flight speed (Fig. 3). The continuous variation in circulation with flight speed suggests a commensurate continuous change in wake geometry, which echoes previous findings for birds (*8*, *10*, *13*), and also parallels the continuous change in wing kinematic parameters with varying flight speed in this (*19*) and other (*14*, *16*, *17*) bat species. The measure Γ/Uc, where c is the mean chord, can be interpreted as half the time-averaged lift coefficient (*13*). Under steady conditions, fixed wings of similar aspect ratio and at similar Re can generate lift coefficients up to about 1.6 (*24*), and because $2\Gamma/Uc$ measured for our bats reached values greater than 4 at 1.5 m/s (Fig. 3), it is likely that some unsteady high-lift mecha-

nism is involved at slow speeds (*25*). Also, when U = 1.5 m/s, for example, St (*22*) was approximately 0.8, a comparatively large number that also argues for the importance of unsteady mechanisms (*19*, *26*).

Previous studies on birds showed that the circulation of the primary start or stop vortices alone was insufficient to support the bird's weight at slow speed (*4*, *5*, *8*, *10*, *13*). However, when the additional positive vorticity shed at the transition between down- and upstroke and into the following upstroke was included in the calculation (*8*, *10*, *13*), an approximate (vertical) force balance could be obtained for birds. Following these calculations, we may compare the total wake circulations with a nominal value Γ_1 that would be required if the wake were composed solely of elliptical loops generated during the downstroke (*20*). As in the bird measurements, calculations where the observed circulation Γ_{obs} was confined to main start/stop vortices showed an insufficient wake vortex strength for weight support at 1.5 m/s [$\Gamma_{obs}/\Gamma_1 = 0.23 \pm 0.05$ (mean ± SD) for both individuals]. Only when Γ_{obs} explicitly includes all the diffuse traces of same-signed vorticity (Fig. 1, D to F) does the ratio of measured to required circulation approach 1 [$\Gamma_{obs}/\Gamma_1 = 0.77 \pm 0.17$ (n = 30 observations) and 0.83 ± 0.18 (n = 23 observations)] for both bats. These values are still below 1 ($P < 0.001$, t test) because the upstroke generates lift not accounted for by Γ_1 (Fig. 1, A, B, H, I, and K). Therefore, the wakes of these bats cannot be adequately described by single discrete vortex loops, and the difference due to the aerodynamically active upstroke is more prominent than in the birds studied so far.

Our flow visualization studies demonstrate how the wake signature changes with flight speed and that the upstroke generates a combined lift and thrust at slow speed. These findings support previous hypotheses based on wingbeat kinematics (*14*–*19*, *27*). The upstroke of these bats also generated useful lift at higher speeds but with different mechanisms. At slow speeds, the wing circulation is reversed, whereas at medium and high speeds it has the same sense during both downstroke and upstroke. The circulation drops to 0 at the transition between up- and downstroke, which contrasts with the constant-circulation wake model for birds at cruising speed (*7*, *8*). Our data also provide evidence for a negative lift during the end of the upstroke at medium and high speeds due to rotation (pronation) and a negative angle of attack of the outer wing at this phase (*14*) (fig. S4). This negative lift may be a constraint due to the use of membranous wings, which cannot separate like the wing feathers of birds. Another difference from birds is that here the circulation varies along the wing span (Fig. 1, D to F). Therefore, neither the simple idealized wake models (discrete loops or constant circulation with partially flexed upstroke) nor the more complex patterns based on detailed bird flight measurements (*8*) are directly applicable. Although the wake properties of this bat species

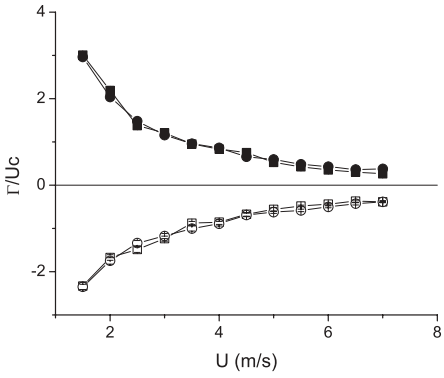

Fig. 3. Variation in circulation Γ of the strongest starting (positive) and stopping (negative) vortices with flight speed (U) for two bats. Γ is nondimensionalized by the mean wing chord c and U. Bat 1 (black squares, start; white squares, stop) and bat 2 (black circles, start; white circles, stop) show statistically indistinguishable values (analysis of variance). Error bars show ± 1 SE.

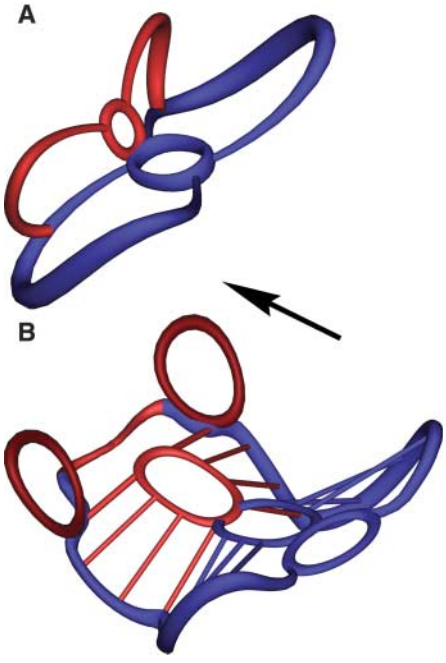

Fig. 4. Cartoons of the (**A**) slow speed (1.5 m/s) and (**B**) medium speed (4 m/s) wakes. Blue denotes vortex structures originating from the downstroke; red from the upstroke. The arrow indicates the flight direction. The slow speed wake has separate vortex loops close to the wing/body junction and a strong signature from the upstroke in red. The medium speed wake has a more continuous shedding of vorticity into the wake, together with reversed-sense vortices produced by the outer wing at the end of the upstroke. This wake also has separate structures shed from the wing roots. The wake at 6.5 m/s (not shown) differs from the wake at 4 m/s by having a longer wavelength, but is otherwise similar. Alternative views are given in fig. S5.

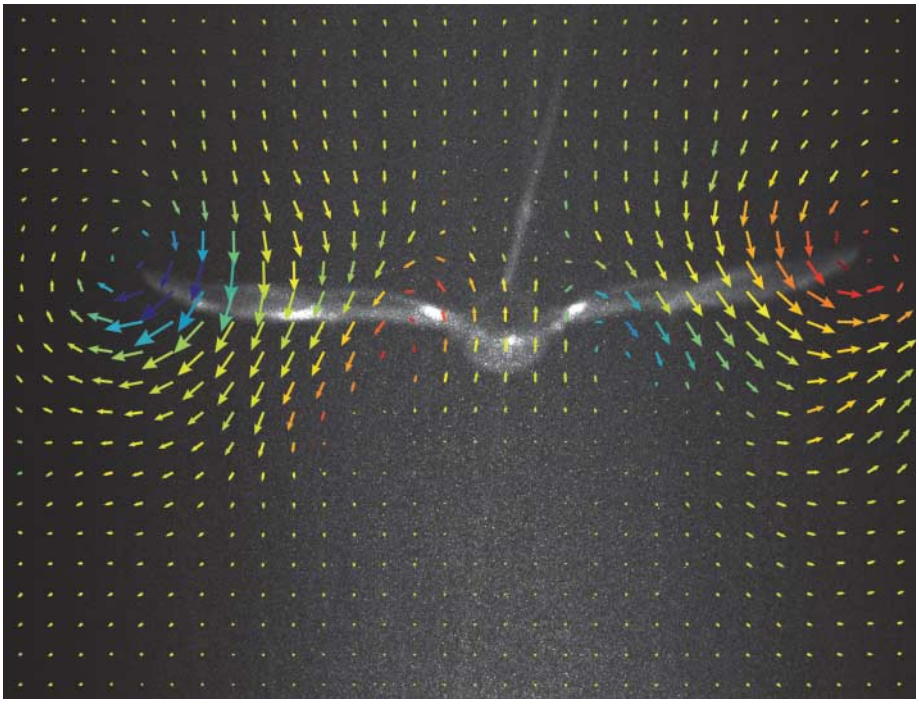

Fig. 2. Velocity field from the transverse (y-z) plane, with a phase- and parallax- corrected image of the bat as seen flying in front of the image plane. The example is from mid-downstroke at 4 m/s, where the two wingtip vortices are clearly seen framing a central induced downwash along the wing's trailing edge. Weaker vortices of opposite sense appear at the wing roots. The colors of the flow vectors indicate the streamwise vorticity magnitude and sign (blue, clockwise and negative; red, anticlockwise and positive).

differ in important ways from those of all previously studied passerine birds, the generality of the result is not yet clear. Kinematic parameters vary between different species of bats (*17*), including the presence of features such as the upstroke reversal found in *G. soricina* (*19*). However, based on the similarities among bat species in the variation of wingbeat kinematics with flight speed (*17*), we may predict the presence of similar features in future bat studies.

From the combined evidence of the two perpendicular image planes (Fig. 1 and fig. S3), together with quantitative measures of the vortex sizes and strengths at different stages of the wingbeat and at different spans, we propose conceptual wake models for example flight speeds of 1.5 m/s (low) and 4 m/s (medium) as shown in Fig. 4. These are not discrete models for each speed but are simply representatives from a continuum across the speed range (Fig. 3). The data show that the aerodynamic wake signature is much more complicated than previous flow visualization studies had suggested (*6*), which is due to the higher-spatial-resolution technique we used. The wake models of Fig. 4 suggest how a new vortex-based aerodynamic model of bat flight could be constructed. Future experiments may investigate the detailed flow on the flexible-membrane bat wing itself to establish the link between the lift-generating mechanism and the resulting wake properties reported here. Those results can further be compared with numerical simulations of appropriate model problems in flexible wing aerodynamics (*28*).

References and Notes

1. Re = Uc/ν (where U is the flight speed, c is the mean chord length in the flightwise direction, and ν is the kinematic viscosity) is a measure of the relative importance of inertial forces to viscous forces. For small birds and bats, Re = 5×10^3 to 30×10^3.
2. S. M. Swartz, M. S. Groves, H. D. Kim, W. R. Walsh, *J. Zool.* **239**, 357 (1996).
3. N. V. Kokshaysky, *Nature* **279**, 146 (1979).
4. G. R. Spedding, J. M. V. Rayner, C. J. Pennycuick, *J. Exp. Biol.* **111**, 81 (1984).
5. G. R. Spedding, *J. Exp. Biol.* **125**, 287 (1986).
6. J. M. V. Rayner, G. Jones, A. Thomas, *Nature* **321**, 162 (1986).
7. G. R. Spedding, *J. Exp. Biol.* **127**, 59 (1987).
8. G. R. Spedding, M. Rosén, A. Hedenström, *J. Exp. Biol.* **206**, 2313 (2003).
9. D. R. Warrick, B. W. Tobalske, D. R. Powers, *Nature* **435**, 1094 (2005).
10. A. Hedenström, M. Rosén, G. R. Spedding, *J. R. Soc. Interface* **3**, 263 (2006).
11. L. Prandtl, O. G. Tietjens, *Fundamentals of Hydro- and Aeromechanics* (Dover, New York, 1957).
12. L. Prandtl, O. G. Tietjens, *Applied Hydro- and Aeromechanics* (Dover, New York, 1957).
13. M. Rosén, G. R. Spedding, A. Hedenström, *J. R. Soc. Interface*, 10.1098/rsif.2007.0215 (2007).
14. U. M. Norberg, *J. Exp. Biol.* **65**, 179 (1976).
15. U. M. Norberg, *J. Exp. Biol.* **65**, 459 (1976).
16. H. D. J. N. Aldridge, *J. Exp. Biol.* **126**, 479 (1986).
17. H. D. J. N. Aldridge, *J. Exp. Biol.* **130**, 275 (1987).
18. O. Von Helversen, in *Bat Flight, Biona Report 5*, W. Nachtigall, Ed. (Gustav Fischer, Stuttgart, Germany, 1986), pp. 107–128.
19. U. M. Lindhe Norberg, Y. Winter, *J. Exp. Biol.* **209**, 3887 (2006).
20. See supporting material on *Science* Online.
21. Aspect ratio (AR) = b^2/S (where b is wing span and S is wing area) is a measure of the wing shape. A high AR indicates a relatively long and slender wing, whereas a small AR signals a short and broad wing.
22. St = fA/U, where f is wingbeat frequency, A is tip-to-tip amplitude of the wingbeat, and U is flight speed relative to the air. St measures the relative magnitudes of wingtip and forward flight speed and can be interpreted as an indicator of the relative unsteadiness and efficiency of the vortex generation. In this study, St = 0.27 at U = 6.5 m/s, 0.37 at 4 m/s, and 0.81 at 1.5 m/s.
23. Y. Winter, *J. Exp. Biol.* **202**, 1917 (1999).
24. E. V. Laitone, *Exp. Fluids* **23**, 405 (1997).
25. Alternatively, using the speed of the wingtip (4.41 m/s at U = 1.5 m/s) yields a conservative estimate of the lift coefficient at C_L = 2.1, which is still considerably larger than 1.6. Furthermore, a truly local force coefficient would be based on the small local wing strip area and would be much higher.
26. G. K. Taylor, R. L. Nudds, A. L. R. Thomas, *Nature* **425**, 707 (2003).
27. S. M. Swartz, K. Bishop, M.-F. Aguirre, in *Functional and Evolutionary Ecology of Bats*, A. Zubaid, G. F. McCracken, T. H. Kunz, Eds. (Oxford Univ. Press, New York, 2006), pp. 110–130.
28. Y. Lian, W. Shyy, *J. Aircraft* **42**, 865 (2005).

29. We thank T. Alerstam for his support and comments on the manuscript. This work was supported by grants from the Swedish Research Council, the Swedish Foundation for International Cooperation in Research and Higher Education, the Knut and Alice Wallenberg Foundation, the Crafoord Foundation, the Magnus Bergvall Foundation, the Royal Physiographical Society in Lund, and the Volkswagen Stiftung.

Supporting Online Material

www.sciencemag.org/cgi/content/full/316/5826/894/DC1
Materials and Methods
Figs. S1 to S5
References

8 March 2007; accepted 4 April 2007
10.1126/science.1142281

The After-Hours Mutant Reveals a Role for Fbxl3 in Determining Mammalian Circadian Period

Sofia I. H. Godinho,[1]* Elizabeth S. Maywood,[2]* Linda Shaw,[1]* Valter Tucci,[1] Alun R. Barnard,[1] Luca Busino,[3] Michele Pagano,[3] Rachel Kendall,[1] Mohamed M. Quwailid,[1] M. Rosario Romero,[1] John O'Neill,[2] Johanna E. Chesham,[2] Debra Brooker,[1] Zuzanna Lalanne,[1] Michael H. Hastings,[2] Patrick M. Nolan[1]†

By screening *N*-ethyl-*N*-nitrosourea–mutagenized animals for alterations in rhythms of wheel-running activity, we identified a mouse mutation, after hours (*Afh*). The mutation, a $Cys^{358}Ser$ substitution in Fbxl3, an F-box protein with leucine-rich repeats, results in long free-running rhythms of about 27 hours in homozygotes. Circadian transcriptional and translational oscillations are attenuated in *Afh* mice. The *Afh* allele significantly affected Per2 expression and delayed the rate of Cry protein degradation in Per2::Luciferase tissue slices. Our in vivo and in vitro studies reveal a central role for Fbxl3 in mammalian circadian timekeeping.

Circadian rhythms, oscillations with a period of ~24 hours, are vital for physiological and behavioral homeostasis in multi- and unicellular organisms. In mammals, these biological rhythms are generated by several genetic elements that form autoregulatory transcriptional and translational feedback loops (*1*–*4*). For the clock to function effectively, however, the phase and extent of protein expression must also be tightly regulated. Posttranslational modifications necessary for the accurate timekeeping of this molecular machinery have been described. For example, Per levels depend on phosphorylation by Doubletime in *Drosophila* (*5*) or casein-kinase Iε in mammals (*6*), and sumoylation is a regulator of Bmal1 function (*7*). Circadian roles for ubiquitin E3 ligases containing F-box motifs (*8*) have been described in *Drosophila* for Slimb (*9*) and JETLAG (*10*) and in *Arabidopsis* for ZEITLUPE (*11*, *12*) and FKF1 (*13*). Large families of mammalian F-box proteins have been identified (*14*–*16*), but, apart from mammalian orthologs of *Drosophila* Slimb (β-TRCP) in cultured cells (*17*), none are known to degrade clock proteins in mammals.

To identify previously unknown genetic factors affecting mammalian circadian behavior, we conducted *N*-ethyl-*N*-nitrosourea (ENU) screens for alterations in circadian wheel-running activity in mice (*18*). We identified one mouse with a circadian period (τ_{DD}) of ~24 hours, significantly longer than the population mean (23.63 hours). The phenotype was inherited in a dominant fashion, with τ_{DD} ranging from 23.9 to 24.3 hours. Intercrosses revealed an additional phenotype with a τ_{DD} of ~26.5 hours and a delay in the entrainment phase angle (Fig. 1A). Frequency distribution plots of backcross (n = 264) and intercross progeny (n = 73) indicated semidomi-

[1]Medical Research Council (MRC) Mammalian Genetics Unit, Harwell, Oxfordshire OX11 0RD, UK. [2]MRC Laboratory of Molecular Biology, Neurobiology Division, Hills Road, Cambridge CB2 2QH, UK. [3]Department of Pathology, NYU Cancer Institute, New York University School of Medicine, 550 First Avenue, MSB 599, New York, NY 10016, USA.
*These authors contributed equally to this work.
†To whom correspondence should be addressed. E-mail: p.nolan@har.mrc.ac.uk